Surface Potential of DPPC Monolayers on Aqueous Solutions at Atmospherically-Relevant Concentrations

Undergraduate Research Thesis

Presented in Partial Fulfillment of the Requirements for Graduation
"with Honors Research Distinction in Chemistry" in the Undergraduate Colleges
of The Ohio State University

by

Clayton B. Casper

The Ohio State University

May 2015

Project Advisor:
Dr. Heather C. Allen
Department of Chemistry & Biochemistry

Abstract

Here the surface potential of DPPC monolayers, a phospholipid found in the sea surface microlayer (SSML), is measured on various salt subphases in an attempt to elucidate the organization of DPPC on air/aqueous interfaces found on marine aerosols. The surface potential results suggest that metal ion binding to the phosphate located in the DPPC head group play an important role in DPPC monolayer organization. For monolayers on subphases containing monovalent cations Na^+/K^+, a small increase (~20−40 mV) in the surface potential with respect to DPPC on neat water is observed. For monolayers on subphases containing divalent cations Mg^{2+}/Ca^{2+} a larger increase in the surface potential (~70−170 mV) is observed. These rises in surface potential are discussed in terms of changing DPPC dipole moments $\Delta\mu_{head}$ and $\Delta\mu_{tail}$ with respect to the surface normal, the packing ability of the monolayer, saturation effects, and the surface potential contribution (Ψ_0) of the electrical double layer (EDL). A 1:1 binding of monovalent cations to phosphate is thought to expand the monolayer by changing the tilt angle of the head group, whereas a 2:1 bridging complex is proposed to explain the increase in surface potential on divalent subphases. Mg^{2+} results agree well with this model. DPPC monolayer results on $CaCl_2$ subphases agree only partially with the bridging model and need to be further explored.

Acknowledgements

I would like to thank my advisor Dr. Heather C. Allen for supporting me in my research goals and giving me advice not only for my present project but my future beyond Ohio State as well. Special thanks go to Ohio State's Office of Undergraduate Education, the Undergraduate Research Office, and the Arts & Sciences Honors Program for financial support during my project. I would also like to thank the Allen group, firstly Dr. Dominique Verreault and Dr. Wei Hua who provided me constant mentorship, feedback on my project, answers to my daily questions, and proofreading of my thesis. Secondly, I would like to thank Ellen M. Adams, for letting me use her isotherm data to help interpret my results. Finally, I would like to thank my wonderful family and Katherine E. Wehde for supporting me.

Keywords: surface potential, DPPC, monolayers, ions, aerosols

Table of Contents

Chapter 1: Motivation

1.1 Importance of Atmospheric Aerosols

One of the most important issues challenging scientists today is untangling the chemistry that drives climate change. Recently, atmospheric aerosols and their contribution to climate change have received much attention. Atmospheric aerosol, which is any suspension of liquid or solid within the atmosphere,[1] has a variety of sources. Natural sources of aerosols include volatile organic compounds (VOCs) released from flora, soot and sulfate compounds resulting from volcanic eruptions, mineral dust from land, and sea spray from the ocean's surface. A large amount of aerosols is also generated from human activities such as fossil fuel burning, agriculture, and biomass burning. Once aerosols enter the atmosphere, they undergo many different morphological and chemical changes. Thus their chemical composition, size, and reactivity are complex. The Intergovernmental Panel on Climate Change (IPCC) reported in 2013 that "clouds and aerosols continue to contribute the largest uncertainty to estimates and interpretations of Earth's changing energy budget."[1]

There are many different pathways by which aerosols can influence Earth's climate. The largest contributions to climate are the aerosol direct and indirect effects. Aerosols interact directly with radiation through scattering and absorption. When aerosols scatter, they reduce incoming solar radiation and this leads to cooling. Local cooling also occurs when aerosols instead absorb radiation, however after thermal mixing and redistribution, this has a net warming effect on the Earth. Indirectly, aerosols affect the atmosphere by acting as cloud condensation nuclei, or by being incorporated into existing clouds. The integration of aerosols into clouds results in a higher concentration of smaller droplets in the cloud's composition. This leads to a

higher cloud surface reflectivity, or albedo. This augments the clouds ability to reflect radiation and cool the Earth.[1] Furthermore, the promotion of aerosol nucleation and growth can provide catalytic sites for heterogeneous reactions in the atmosphere. An important example is the release of chlorine radicals from polar stratospheric clouds, which ultimately leads to ozone depletion.[2]

Aerosol effects depend on scattering and absorption cross-sections, hygroscopicity, and uptake coefficients, all of which rely on aerosol chemical composition, and more importantly, the surface properties of particles.

1.2 Marine Aerosols

Of particular interest to this study are marine aerosols, which make up a large portion of the global aerosol emissions in the troposphere. Marine aerosols are formed by mechanical wave action and bubble bursting at the ocean's surface, resulting in a suspension of sea spray into the air and bubble bursting. When a bubble bursts, fragments of the bubble aqueous film are ejected upwards into the air. Additional droplets are produced when they separate from the water jet that results from the force of the bubble burst.[3,4]

Important in these processes is the sea surface microlayer (SSML), which is the thin boundary layer (1−1000 μm)[5] located at the ocean surface and directly in contact with the atmosphere. This layer has been shown to be enriched in organic compounds, such as phospholipids, fatty acids, amino acids, carbohydrates, and sterols.[3,6] These organics derive from living and decaying plankton and bacteria that have risen to the surface. It is believed that the SSML plays a large role in coating marine aerosols with organics as they form.[3,6]

The model for a marine aerosol is that of an inverted micelle (Fig. 1), which is composed of an aqueous core with a single hydrophobic boundary. Marine aerosols have an aqueous brine

center surrounded by an organic layer mostly composed of surface-active compounds, or surfactants.[7,8] The organic layer on these aerosols is mostly hydrophobic. As marine aerosols age, hydroxyl, chlorine, ozone, and NO_3 radicals present in the atmosphere oxidize the organic layer, making it a more hydrophilic and reactive site for heterogeneous reactions and species uptake.[7]

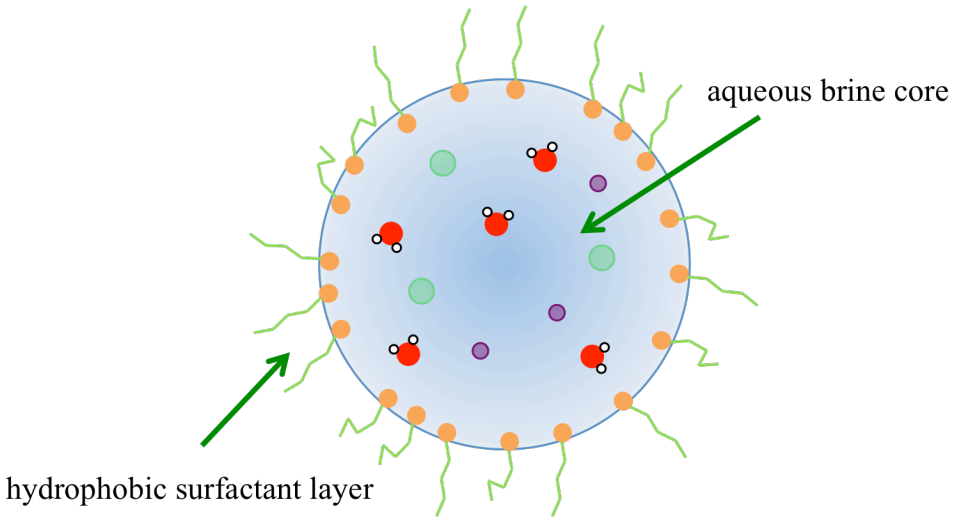

Figure 1. Schematic representation of the inverted micelle model for a marine aerosol: a core containing both water and ions (*green* and *purple*) surrounded by an organic layer (*orange* and *green*).

1.3 Experimental Models for Marine Aerosols

As stated above marine aerosols contain a wide variety of organic compounds at their surface. Studying the role of a single compound in the organic layer can be challenging, because the sample contains a large matrix of other compounds. Nevertheless, fundamental studies of organics found at the surface of marine aerosols can provide insight into the organization of a marine aerosol organic layer.

Many amphiphilic molecules can readily organize themselves into a single layer on a surface, which makes them useful surrogates for studying the surfaces of marine aerosols. One type of

such molecules is phospholipids. Phospholipids are easily found in the ocean, as they compose a large portion of cellular membranes of marine organisms. The most prevalent phospholipids found at the SSML are those with sixteen or eighteen carbon chains[9,10] and phosphate head groups with carboxylic acid and amine moieties.[11]

1.4 Objectives

In this study, the saturated phospholipid dipalmitoylphosphatidylcholine (DPPC) is investigated (Fig. 2). DPPC has two sixteen carbon chains making up the hydrophobic tails, which are attached to a hydrophilic choline head group (i.e., phosphate linked to a *tert*-methylamine group). DPPC monolayers were created and studied using surface potentiometry. DPPC monolayers on neat water and monolayers on salt-containing solutions were compared with the aim of elucidating the organization of DPPC at the interface and the ability of DPPC monolayers to bind with salts. The surface potential is a useful alternative to other surface sensitive techniques such as vibrational sum frequency generation (VSFG) spectroscopy and Brewster angle microscopy (BAM) because the measurement is relatively simple and can provide additional information on the electrical environment at the surface.

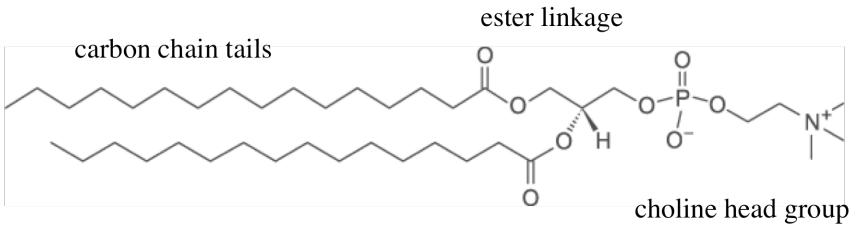

Figure 2. Chemical structure of DPPC.

Chapter 2: Surface Potentiometry and Tensiometry

2.1 Surface Potential Theory

2.1.1 Electric Potential

The electric potential at a point in space is a reflection of the strength of the electric field there. Because both direction and magnitude are important in electrostatics, the electric field is often thought of as a vector field, that is to say, that at each point in space, there is a vector with a direction and a magnitude that describes the electric field. However, the electric potential is a scalar (numerical) field. The equation for the electric potential (V) at any given point P due to a charge Q is given by:

$$V = \frac{1}{4\pi\varepsilon_0}\frac{Q}{r} \tag{1}$$

where r is the distance from the charge Q, and $\varepsilon_0 = 8.854\times10^{-12}$ F/m is the vacuum permittivity. The difference between two electric potentials at different points in space is called an electric potential difference, or voltage.

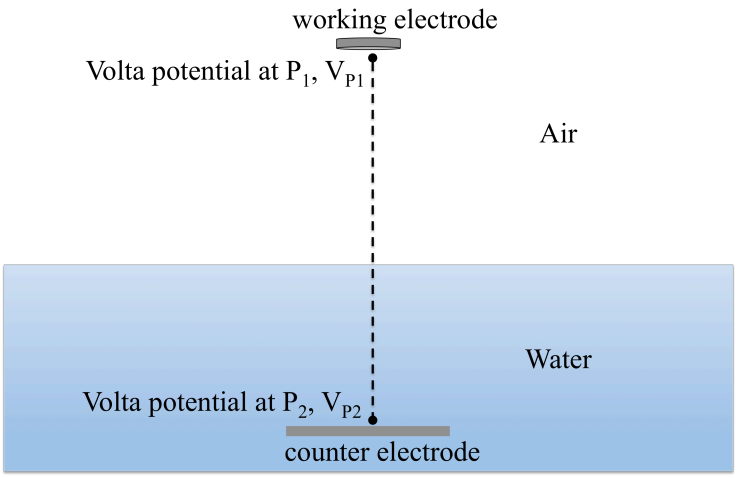

Figure 3. Schematic representation of the Volta potentials at the air-water interface.

Consider two media with different electrical and optical properties separated by a plane interface such as in the case of the air/water interface (Fig. 3). Now, assume two points P_1 and P_2, one in each medium; the potential difference between these two points depends on the electrical properties in each medium and the properties of the boundary separating the two phases. If metal electrodes were used to measure this voltage, then the measurement would depend also on the potentials between the electrode metal and air, and the electrode metal and water. These potential differences are called the Volta potentials, or contact potentials. The voltage between the points shown in Fig. 3 is then the difference between these Volta potentials. This is called the surface potential because the voltage contains information about the boundary or surface between the two points. The surface potential of a bare air/aqueous interface is then given by:

$$\Delta V_{surface} = \Delta V_{air,electrode} - \Delta V_{water,electrode} \tag{2}$$

Typically in an actual experiment, the surface potential of a neat water interface is used as a reference. In this case, the surface potential of the sample system under investigation is written as:

$$\Delta V_{measured} = \Delta V_{sample} - \Delta V_{air/water} \tag{3}$$

2.2 Measurement Methods of the Surface Potential

2.2.1 Vibrating Plate Method

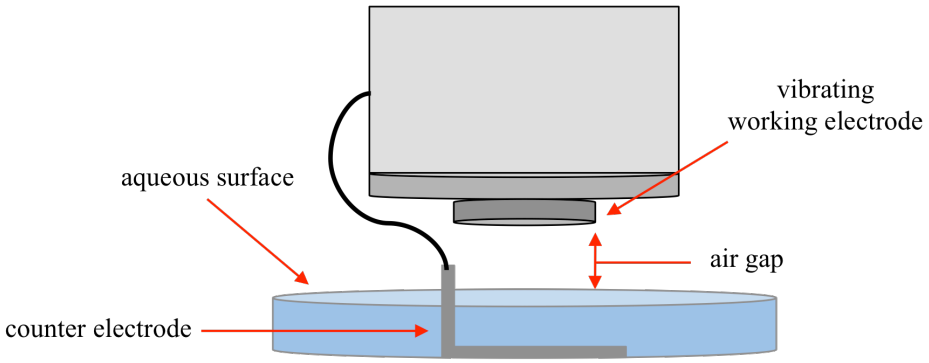

Figure 4. Schematic representation of the vibrating plate method.

One of the most commonly used methods to measure the surface potential at an air/aqueous interface is the vibrating plate (VP) method (Fig. 4). In this method, a vibrating working electrode, usually made of an inert metal such as platinum or stainless steel, is brought in close proximity to the aqueous interface. The working electrode is connected to a counter electrode also made of an inert metal, which sits below the interface, in the bulk aqueous phase. The measuring principle behind this setup is that the working electrode, the interface, and the air between them form a parallel plate capacitor with capacitance defined by:

$$C = \frac{\varepsilon A}{d} \tag{4}$$

where ε is the relative permittivity of the dielectric between the plates, A is the area of the plates, and d is the distance them.

Thus, the capacitance of the system is dependent on the distance between the working electrode and the aqueous surface. When the working electrode is vibrating at a constant frequency ω, the air gap distance continually changes by small amounts. Then, the capacitance C can be described by a time-harmonic profile such as

$$C = C_0 + C_1 \sin \omega t \tag{5}$$

where C_0 is the capacitance when the vibrating plate is at rest and C_1 represents the greatest contribution to the capacitance during vibration.

Electronically, the surface potential ΔV is found using a null-point detection method. The time-harmonic capacitance creates an alternating current, which is then amplified and integrated into a voltage (Fig. 5). This voltage, called the compensating voltage or (ΔV_{comp}), is fed back into the circuit. This loop continues, until the alternating current produced is zero. The voltage measured across the interface is then the compensating voltage.[12]

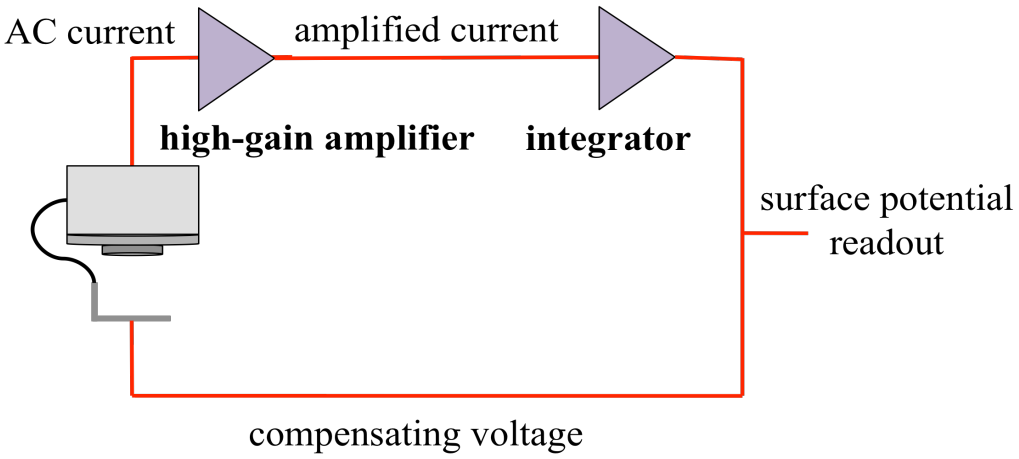

Figure 5. Simplified circuit for the VP method.

2.2.2 Limitations and Drawbacks of the VP Method

As mentioned above, the surface potential measured is created from the capacitor formed between the aqueous surface and the working electrode. The capacitance is strongly dependent on the air gap, which is typically 1−2 mm. In experiments with aqueous surfaces, the surface potential of the system of interest is measured against a neat water reference. Thus the replacement of the reference solution with the sample solution is a difficult and critical step. The removal of solution can be done by utilizing an aspirator, or another vacuum suction, but it

introduces the risk of generating stray capacitances if the suction tip nears the electrode. However, the error introduced by such capacitances has been reported to be on the order of tenths of mV,[12] which may be negligible for some experiments. Regardless of the replacement method, it is important to maintain a constant air gap distance throughout measurement.

Furthermore, stray electrical charges can influence the measurement. Static charge can build on any part of the setup, which could lead to spurious potential drops, influencing the stability of the potentiometer. In order to minimize these disturbances, the surface potentiometer is typically housed in a grounded Faraday cage with humidity control.

2.2.3 Ionizing Electrode Method

Another major method for measuring the surface potential is the ionizing electrode (IE). Similar to the VP method, this method treats the system as a parallel plate capacitor but the working electrode is no longer a vibrating plate, but rather an electrode with a small radiation source. The radiation source is usually an α-emitter that can produce a large amount of ionization over a small distance. A typical ionizing source used in the IE method is Am^{241} which has a strong alpha emission and a half-life of ~433 years. Like the VP plate method, the IE has been used to measure the surface potential of electrolyte solutions and lipid monolayers.[13,14]

2.3 Models of the Surface Potential on Lipid-Covered Aqueous Interfaces

2.3.1 Contributions to the Surface Potential of Lipid Monolayers

The surface potential of a lipid-covered aqueous surface is influenced by a variety of factors, such as interfacial water organization, monolayer properties, and surface concentrations of

species in the subphase. The surface potential measured in experiment can be broken down into three terms:

$$\Delta V = \Delta V_0 + \Delta V_P + \Psi_0 \tag{6}$$

where ΔV_0 is the measured surface potential of the reference (e.g., bare air/aqueous interface), ΔV_P is the dipole contribution of the monolayer, and Ψ_0 is the contribution of the electrical double layer formed by the distribution of charges at the surface.

2.3.2 Models of the Monolayer Dipole Contributions

One of the earliest and simplest models of lipid monolayer contributions to the surface potential is the one of Helmholtz which treats the monolayer as a collection of dipoles floating at the surface, thus forming a parallel plate capacitor.[15] The surface potential is given by the Helmholtz equation:[16]

$$\Delta V_P = \frac{\mu_\perp}{A\varepsilon_0} \tag{7}$$

where A is the mean molecular area (in Å^2/molecule), ε_0 is the vacuum permittivity, and μ is the component of the net molecular dipole moment that is normal to the surface (Fig. 6). The Helmholtz model predicts lower dipole moments than dipoles measured in experiments,[17] suggesting that there are contributions that this equation does not take into account.

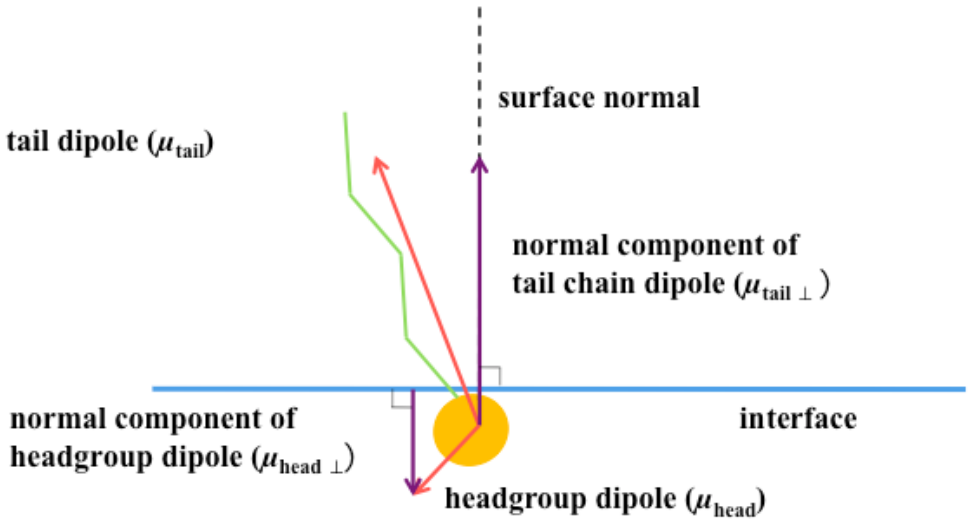

Figure 6. Schematic representation of the net molecular dipole of a single lipid and its component normal to the surface.

Later Demchak and Fort tried to expand the Helmholtz model by hypothesizing that the dipole reflected in the surface potential of monolayers is a sum of three contributing factors: the dipole moment of the lipid tail group, the lipid head group, and the reorganization of interfacial water due to the monolayer:[18]

$$\Delta V_P = \frac{1}{A\varepsilon_0}\left(\frac{\mu_{tail}}{\varepsilon_{tail}} + \frac{\mu_{head}}{\varepsilon_{head}} + \frac{\mu_{water}}{\varepsilon_{water}}\right) \tag{8}$$

where μ_i and ε_i (i = tail, head, water) represent the normal dipole moments and local dielectric constants in each particular region. The dielectric constants are hard to determine in practice and it is assumed that they do not change in a monolayer. However, it has been shown that some of these constants, such as ε_{tail} and ε_{head}, can be approximated with DFT calculations paired with experimental surface potential data.[19] In contrast, it is possible to calculate the dipole moments of the tail and head groups, μ_{tail} and μ_{head}, through carefully designed experiments. Partial dipole compensation is one example of such experiments.[20] In this design by Vogel and Möbius, the surface potential of two lipid monolayers was compared (Fig. 7). The lipids that compose

monolayer A have a single head group attached to an alkyl hydrophobic tail. If one assumes the bonds in the alkyl chain are all *trans* (which is reasonable for condensed phases), the normal dipole moment of the tail μ_{tail} depends only on the dipole terminal $-CH_3$ group. Lipids in monolayer B contain the same head group and tails as lipids in monolayer A, but each lipid molecule has two head groups. Monolayer B also contains unattached alkyl chains, which have two terminal $-CH_3$, but no headgroup. The dipole contribution of the head group in monolayer A is the same as that of monolayer B. However, because of the compensation of the unattached tails in monolayer B, the tail dipole contribution differs between the two monolayers. The difference in surface potential of these two monolayers can then give an experimental value of μ_{tail}. This is just one example of how the Demchak-Fort model could be useful for quantifying experimental surface potential data for molecular dipoles or vice-versa.

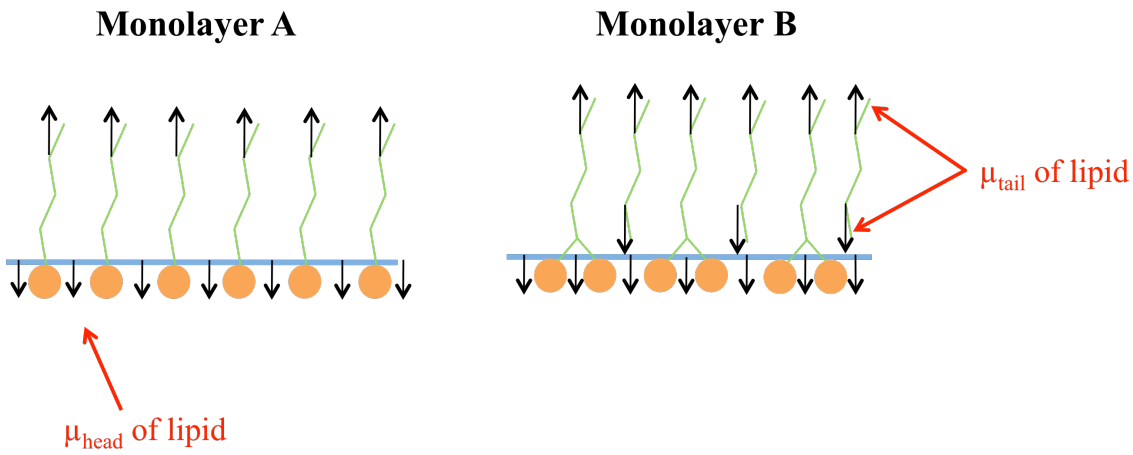

Figure 7. Schematic representation of the partial dipole compensation experiment.

2.3.3 Gouy-Chapman Model of the Electrical Double Layer Contribution

In aqueous solutions, some ions have a propensity to be at or near the interface. The concentration and distribution of these ions in the interfacial region can not only affect the surface potential through electrostatic interactions with the monolayer, but also through shielding

with what is called the electrical double layer (EDL) (Fig. 8). For ionic solutions, this model hypothesizes that ions exist underneath a monolayer, balancing any charges present in the head group region. In addition, a counterion layer is formed underneath the previous layer in a further effort to balance charge. The contribution from this EDL (Ψ_0) can be calculated from a model proposed by Gouy and Chapman:[21]

$$\Psi_0 = \frac{2k_BT}{e}\sinh^{-1}\left(\frac{-\sigma}{\sqrt{8\varepsilon_0\varepsilon N_A k_B T c}}\right) \tag{9}$$

where σ is the surface charge density of the monolayer, ε_0 is the vacuum permittivity, ε is the dielectric constant of the aqueous phase, k_B = 1.3806×10^{-23} J/K is Boltzmann's constant, N_A = 6.022×10^{23} mol^{-1} is Avogadro's number, and c represents the concentration of ions in the subphase.

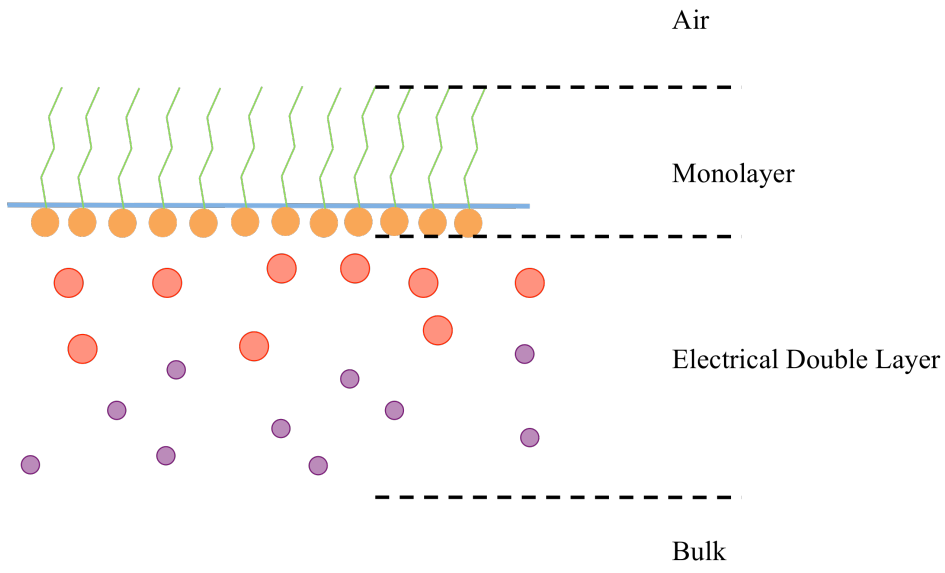

Figure 8. Schematic representation of the EDL near a charged lipid-covered aqueous surface. Charge is not specified for ions (*red*) and co-ions (*purple*).

When dealing with solutions that have divalent (doubly-charged) ions, the concentration term c should be replaced with ionic strength I:

$$I = \frac{1}{2}\sum_{i=1}^{n} c_i z_i^{\,2} \tag{10}$$

where c_i and z_i are the bulk molar concentration and charge of the i-th ionic species There are some limitations of this model. The model works best with monolayers of large areas (a suggested lower limit is 85 $Å^2$ per ionized molecules).[21] For DPPC, the liquid-expanded phase ends at around 80 $Å^2$/molecule which suggests that EDL quantification at smaller area phases (coexistence or liquid-condensed phase) will not be accurate. Eq.(9) is not meant to be a rigorous model of the EDL, but rather an outline of electrostatic considerations. The variety of factors involved with a realistic depiction of the EDL – surface charge densities, ion size, charge, concentration, ion-ion correlations, and interactions between ions and the monolayer – complicate a working model on the electric environment near the interface. It is still useful, however, to use the model as an estimation of ionic effects on the measured surface potential.

2.4 Surface Tensiometry

Another common technique used to study monolayers is surface tensiometry. There are several methods to measure the surface tension of a liquid. In the Wilhelmy plate method (Fig. 9), a plate made of platinum, stainless steel, or ashless filter paper is suspended from a balance into the liquid so that only a small portion of the plate is immersed. The resulting force acting on the plate in this configuration is a balance between gravitational forces, pulling downwards, and both buoyancy and surface tension, both acting upwards:[15]

$$F = \rho_p glwt + 2\gamma(t + w)\cos\theta - \rho_l gtwh \tag{11}$$

where *l, w, t* are the dimensions (length, width, thickness respectively) of the Wilhelmy plate, made of a material with density ρ_p and at height *h*, γ is the surface tension of the liquid, and θ is the contact angle between the plate and the liquid surface (Fig. 10). It is assumed that the Wilhelmy plate is completely wetted with a contact angle of ~0º and the thickness of the plate is negligible. In the case of a monolayer, the change in the surface tension from a neat water reference can be determined through the change in force measured by the balance:

$$\Delta\gamma = \frac{\Delta F}{2w} \tag{12}$$

The change in surface tension is called the surface pressure Π:

$$\Pi = \Delta\gamma = \gamma_{monolayer} - \gamma_{water} \tag{13}$$

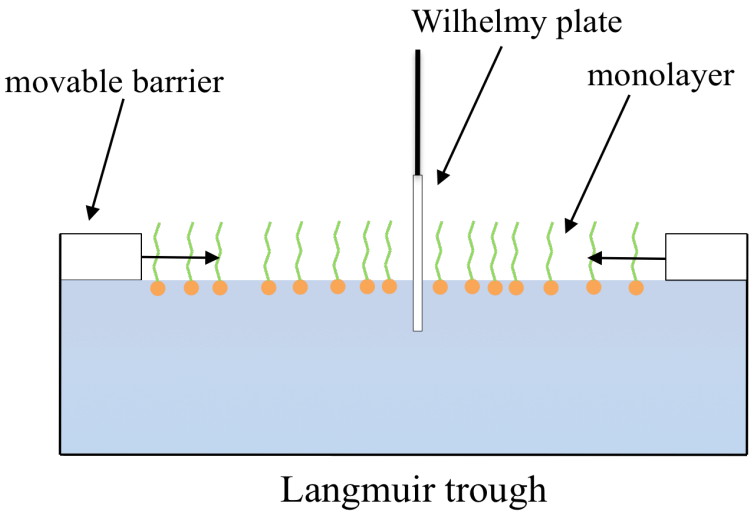

Figure 9. Schematic representation of the Wilhelmy plate method to measure surface tension (side view).

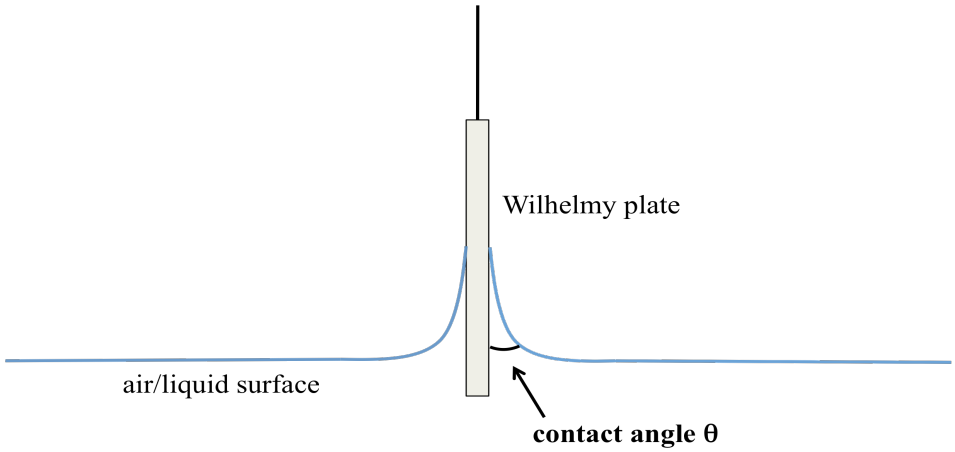

Figure 10. Schematic representation of the contact angle θ made between the Wilhelmy plate and the liquid surface.

Typically in surface tensiometry experiments, the trough will feature movable barriers. These barriers serve to compress the monolayer, increasing the surface pressure and thus allowing measurement in different lipid phases. An example of an isotherm obtained by the Wilhelmy plate method on a DPPC monolayer spread on water is shown in Fig. 11. Surface pressure is usually plotted against mean molecular area (in units $Å^2$/molecule), which is a measure of how much area each lipid molecule covers on the surface.

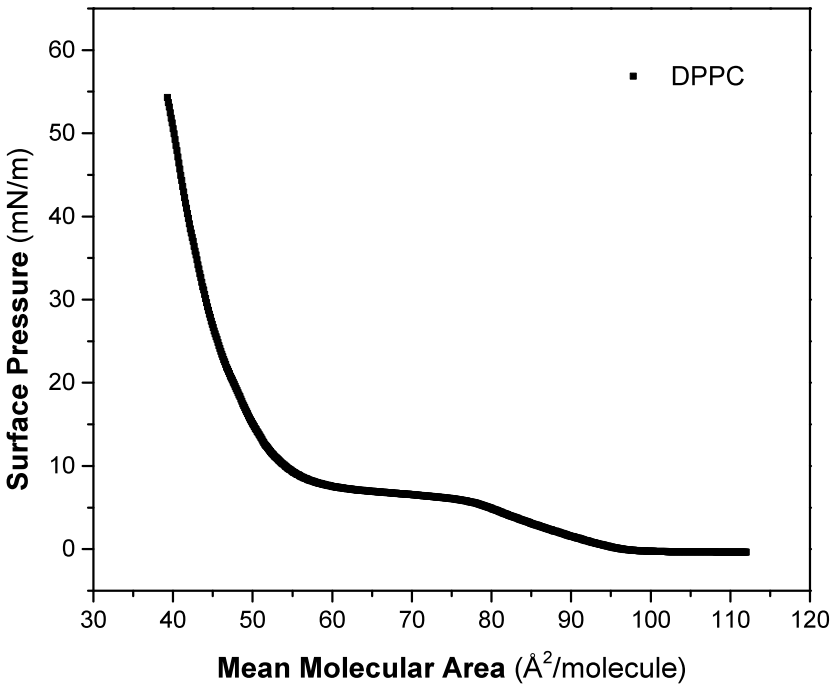

Figure 11. Example of a surface pressure–mean molecular area per molecule (Π-*A*) isotherm of a DPPC monolayer spread on water.

Chapter 3: Materials and Methods

3.1 Materials

NaCl (≥99%, ACS certified crystalline), KCl (≥99%, ACS certified crystalline), $MgCl_2 \cdot 6H_2O$ (≥99%, ACS certified crystalline), $CaCl_2 \cdot 2H_2O$ (≥99%, ACS certified crystalline) were obtained from Fisher Scientific (Waltham, MA). DPPC was purchased from Avanti Polar Lipids (Alabaster, AL) and then dissolved in chloroform (HPLC grade, Fischer Scientific). Ultrapure water with a resistivity of 18.2–18.3 MΩ•cm and a pH ~ 5.6 (acidic due to dissolved CO_2 gas) was obtained from a Barnstead Nanopure system (model D4741, Thermolyne Coproration, Dubuque, IA) with additional organic removing cartridges (D5026 Type I ORGANICfree Cartridge Kit; Pretreat feed).

3.2 Preparation of Salt Solutions

Salts were dissolved in ultrapure water and then filtered 2-4 times using carbon-activated filters (Whatman Carbon Cap 75, Fisher Scientific) in order to remove any impurities. The filters were flushed with ultrapure water for 30 min to 1 h before use to remove any residual compounds. The extensive purification of salts is required because it has been shown that organic impurities still exist at the surface for ACS grade salts of ≥ 99% purity.[22] The filtered solutions were then checked using vibrational sum frequency generation (VSFG) spectroscopy in the C-H stretching region (2800−3000 cm^{-1}) for organic impurities. The VSFG spectra showed no peaks associated with C-H stretching modes, indicating that the surfaces of the salt solutions were free of contaminants. The salt solutions were then standardized using the Mohr titration method for the chloride ion.[23] Once the concentrations were known, each salt stock solution was diluted to the following concentrations: 0.6 (0.3 for divalent cations), 1.0, and 2.0 M. The lower

concentration was chosen in order to emulate the typical salt concentration in sea water[24]. The higher concentrations were chosen because once a marine aerosol is in the atmosphere; it may lose water to evaporation and become more concentrated in salts.

3.3 Surface Tension Measurements

Surface pressure–mean molecular are (Π-*A*) isotherms were collected using a Langmuir trough (KSV Minitrough, Biolin Scientific USA, Linthicum Heights, MA). The trough is made of Teflon with dimensions of 168 mm × 85 mm. The monolayer was compressed using barriers coated with Delrin, a hydrophobic material, at a rate of 5mm/min/barrier. During compression, the surface pressure and mean molecular area per molecule were monitored using a Wilhelmy plate balance. The Wilhelmy plate was made out of filter paper (Ashless grade, Whatman, Pittsburg, PA, USA). The trough was rinsed four to six times with ethanol and then ultrapure water respectively before use. The trough was considered clean after barrier compression showed no significant change (< 0.1 mN/m) in surface pressure. After DPPC was spread on the surface, 10 min was allowed for solvent evaporation.

3.4 Surface Potential Setup

The surface potentiometer (SPOT I, Biolin Scientific USA; 140 Hz, ± 3 mV) was shielded by a custom-built Faraday cage (Fig. 12 and 13). The Faraday cage (60 cm (length) × 35 cm (width) × 45 cm (height)) was custom designed using Autodesk Inventor (v. 2014, Mill Valley, CA) and fabricated in the department's machine shop. The cage was built with a copper frame, upon which two layers of copper mesh (TWP Inc., Berkeley, CA; wire diameter 4 mm, opening size < 1 mm) were connected using double-sided carbon tape (SPI Supplies, West Chester; 25 mm × 20 mm on 76 mm plastic core). Small rectangular on the back and side panels were cut to allow

electric wiring. The Faraday cage was enclosed in a Plexiglas box in order to minimize disturbances from air currents and dust particles. The relative humidity of the enclosure was controlled by a large Petri dish containing water placed on a hot plate. The relative humidity varied from 40 to 70%.

The sample cell (88 mm × 44 mm × 10 mm) was made of PTFE and placed on top of a vertical translation stage (Model MVS005/M, ThorLabs, Newton, NJ: 13 mm travel, ±5 μm), in order to ensure reproducible air gap distances.

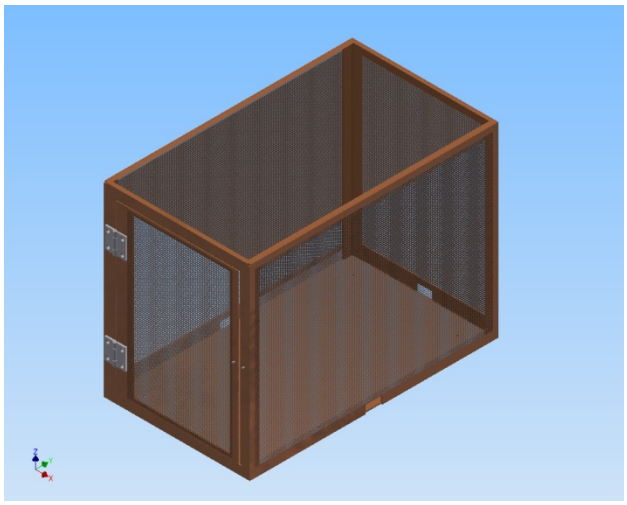

Figure 12. Schematic drawing of the Faraday cage with copper mesh on a copper frame.

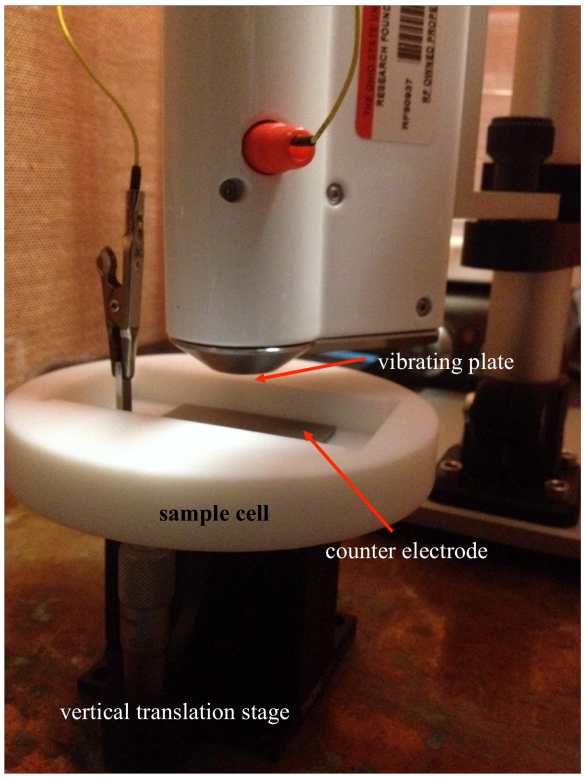

Figure 13. Picture of the surface potential setup with sample cell and surface potentiometer head.

3.5 Surface Potential Measurements

The surface potential of DPPC monolayers on various salt subphases was measured. For all experiments, removal of solution from the cell was done using a vacuum line aspirator with the aspirator tip being changed frequently. The removal is done at a position away from the surface potentiometer. The vertical translation stage is used to lower the cell from the vibrating working electrode and the stage is brought out from underneath the potentiometer. Any cleaning or removal of the water reference is done in this position, after which the cell is returned to underneath the electrode and raised back to the previous height.

Prior to the beginning of each experimental day (Fig. 14), the sample cell was filled with ultrapure water and the potentiometer was "warmed-up" for one hour as recommended by the

manufacturer. Afterwards the surface potential of another ultrapure water sample was recorded for 10 min. The trial begins with this measurement and it is considered the reference or blank value. In the case of trials with salt subphases, the water reference is removed, the surface potential is zeroed, and then the water is replaced with the salt solution. The surface potential of the bare salt aqueous interface is then recorded for 10 min. The monolayer is added to the interface by spreading a DPPC solution using a 10 μL microsyringe (701N, Hamilton, Reno, NV) that has been pre-rinsed five times with chloroform and one time with the DPPC solution. In order to measure the surface potential over each phase of the DPPC monolayer, additions of 0.96 mM DPPC were spread (7.9 μL for liquid-expanded (LE, 81 MMA, 5 mN/m) phase, 2.4 μL for the liquid-expanded-liquid-condensed (LE-LC, 62 MMA, 8 mN/m) coexistence region, and 4.6 μL for the liquid-condensed (LC, 41 MMA, 41 mN/m) phase). After each spreading, a period of 10 min was allowed to let the chloroform evaporate. For each DPPC phase, the surface potential was recorded for 5 min before proceeding to the next. After the LC phase is measured, the cell and counter electrode were cleaned 2 times with ethanol (Reagent alcohol, histological grade, Fisher Scientific) and 8 times with ultrapure water. A typical experimental day comprised this method being repeated for three concentrations of a single salt and one measurement of DPPC on ultrapure water.

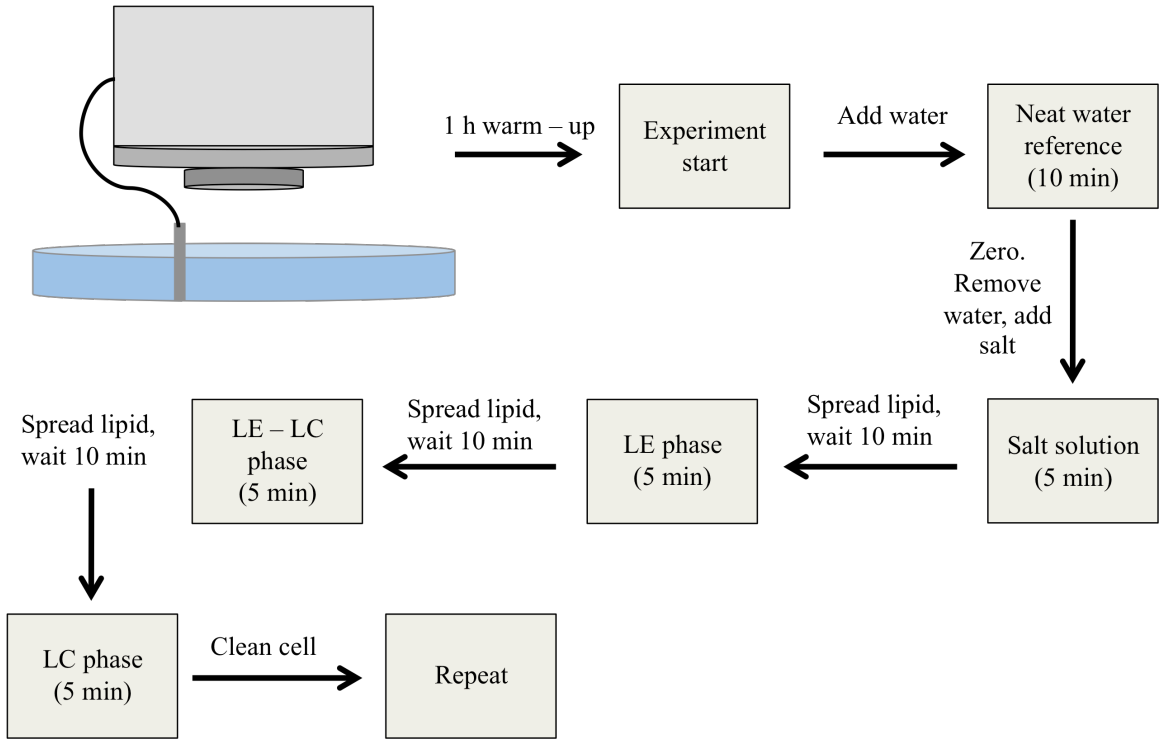

Figure 14. Schematic representation of the general procedure used to measure surface potential on DPPC-covered salt solutions.

Table 1. Surface potential of DPPC monolayers on aqueous salt subphases. Error bars for H_2O are over 12 measurements. Error bars for salts are over 3 measurements.

Subphase	**Concentration** (M)	**Surface Potential** (mV)		
		DPPC Phase		
		LE	LE-LC	LC
H_2O		288 ± 15	324 ± 20	595 ± 13
NaCl				
	0.6	326 ± 6	362 ± 7	562 ± 11
	1.0	324 ± 1	357 ± 5	563 ± 1
	2.0	301 ± 13	344 ± 29	549 ± 25
KCl				
	0.6	334 ± 6	368 ± 8	574 ± 9
	1.0	326 ± 27	360 ± 35	563 ± 23
	2.0	298 ± 28	325 ± 22	534 ± 18
$MgCl_2$				
	0.3	404 ± 13	445 ± 23	666 ± 11
	1.0	418 ± 6	450 ± 8	687 ± 6
	2.0	451 ± 10	497 ± 15	709 ± 14
$CaCl_2$				
	0.3	426 ± 17	480 ± 30	702 ± 25
	1.0	452 ± 30	492 ± 11	734 ± 30
	2.0	388 ± 12	436 ± 26	668 ± 12

Chapter 4: Results and Discussion

4.1 DPPC Isotherms

Two isotherms of the DPPC used in this study are shown in Fig. 15. The lift-off values of DPPC are known to be 96 Å^2/molecule,[25] which are the observed values in the isotherms, once the concentration of DPPC was adjusted to 0.96 mM. From these collected isotherms, it was determined at which mean molecular areas each DPPC phase was occurring. The target MMA values for the surface potential experiments were 80 Å^2/molecule for the LE phase, 60 Å^2/molecule for LE-LC phase, and 40 Å^2/molecule for LC phase.

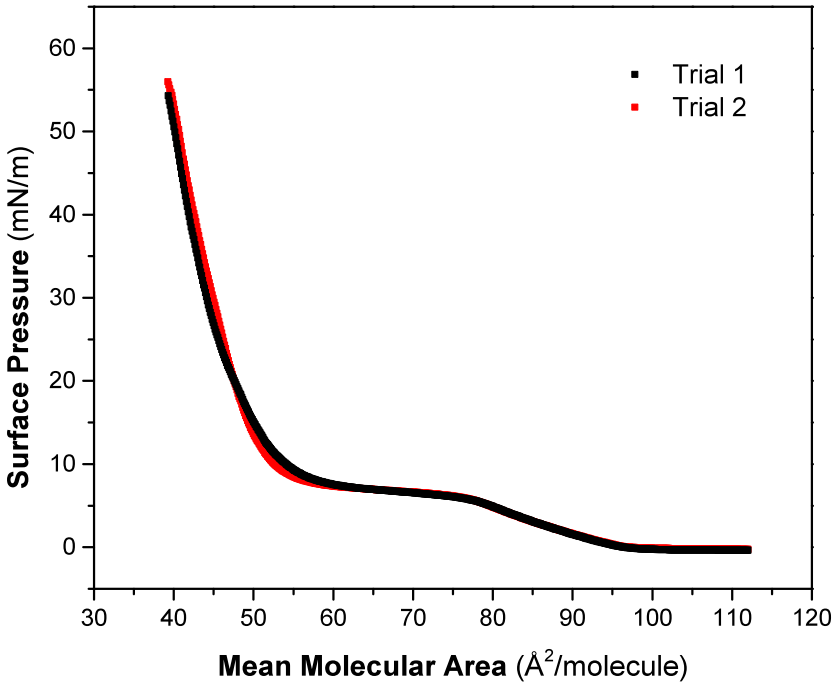

Figure 15. Collected surface pressure-molecular area isotherms of DPPC monolayers spread on water.

4.2 Surface Potential Measurements of DPPC Monolayers on Monovalent Salt Subphases

The surface potential values obtained for the reference DPPC monolayers on neat water agree well with literature as shown in Fig. 16.[26,27] The surface potential comparison between DPPC monolayers on salt subphases and neat water is shown in Table 1 and Fig. 17. DPPC monolayers on Na^+ and K^+ subphases differed slightly from that on neat water. Compared to DPPC monolayers on a neat water surface, monolayers on monovalent salt surfaces show an increase of 20–40 mV in surface potential for the non-condensed phases (LE and LE-LC), but a decrease of 30–60 mV for the LC phase. Interestingly, as the concentration of the salt subphase increased from 0.6 to 1.0 M, the surface potential of the monolayers showed little change, but at 2.0 M it decreased to values below that of the lower concentrations.

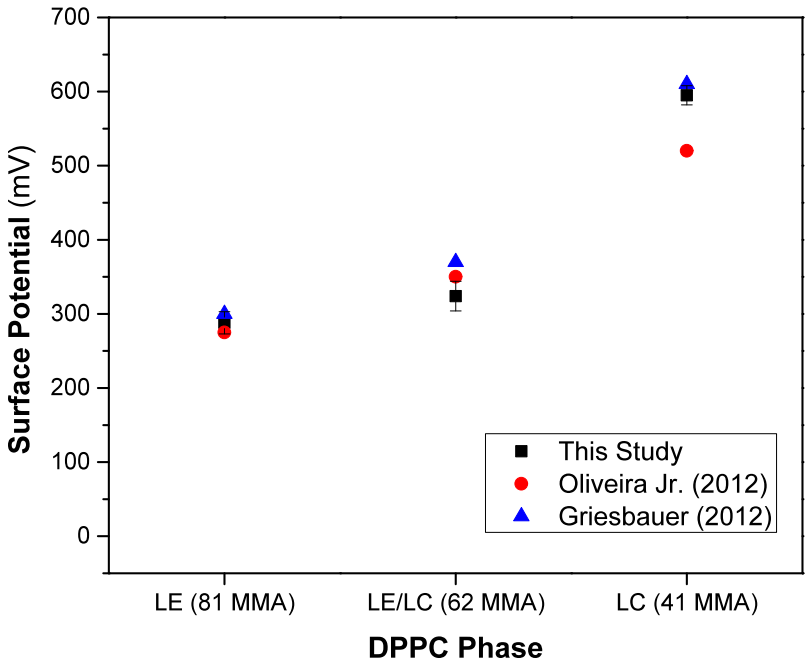

Figure 16. Surface potential of DPPC monolayers on ultrapure water.

The interpretation of the observations described above can be done through Eqs. (6) and (8). That is, the observed surface potential values depend largely on changes in the dipole of the

phospholipid head group μ_{head}, changes in the dipole of the phospholipid alkyl chain tails μ_{tail}, and the contribution from the electrical double layer Ψ_0. These changes are outlined in Fig. 18 below. Since no large differences were observed between the LE and the LE-CE phases with monovalent salts, only the LE phase is discussed.

4.2.1 Surface Potential Contributions in the DPPC LE Phase

In the LE phase, the surface potential of DPPC on water was lower than that measured on Na^+/K^+ salt subphases. The presence of salt changes contributions on all three of the aforementioned terms. The first contribution is changes in the polar head group orientation. In the presence of metal cations, it is thought that the head group lies closer to the interface.[28] This is confirmed in surface pressure-area the Π-*A* isotherms of DPPC, where DPPC has been shown to have larger lift-off areas (at 108 $Å^2$/molecule for 2.0 M NaCl compared to 96 $Å^2$/molecule for neat water) (see Figs. 20 and 21 in the Appendix).[a] Because the area contribution of the chains in the LE phase is relatively low, the lift-off area can be assumed to be an approximation of the head group area. The larger head group area described by these isotherms suggests that the head group sits closer to the surface. This agrees with VSFG studies on DPPC, which observe an angle of ~10º from the surface for the P-N bond in the phosphate-choline head group.[29] It's important to note that μ_{head} points towards the bulk phase, while μ_{tail} points in the opposite direction. Thus the decrease in μ_{head} is a positive contribution to the surface potential, which agrees with the observed increase in surface potential for monovalent salts in the LE phase.

[a] This information was obtained through private communication with Ellen M. Adams.

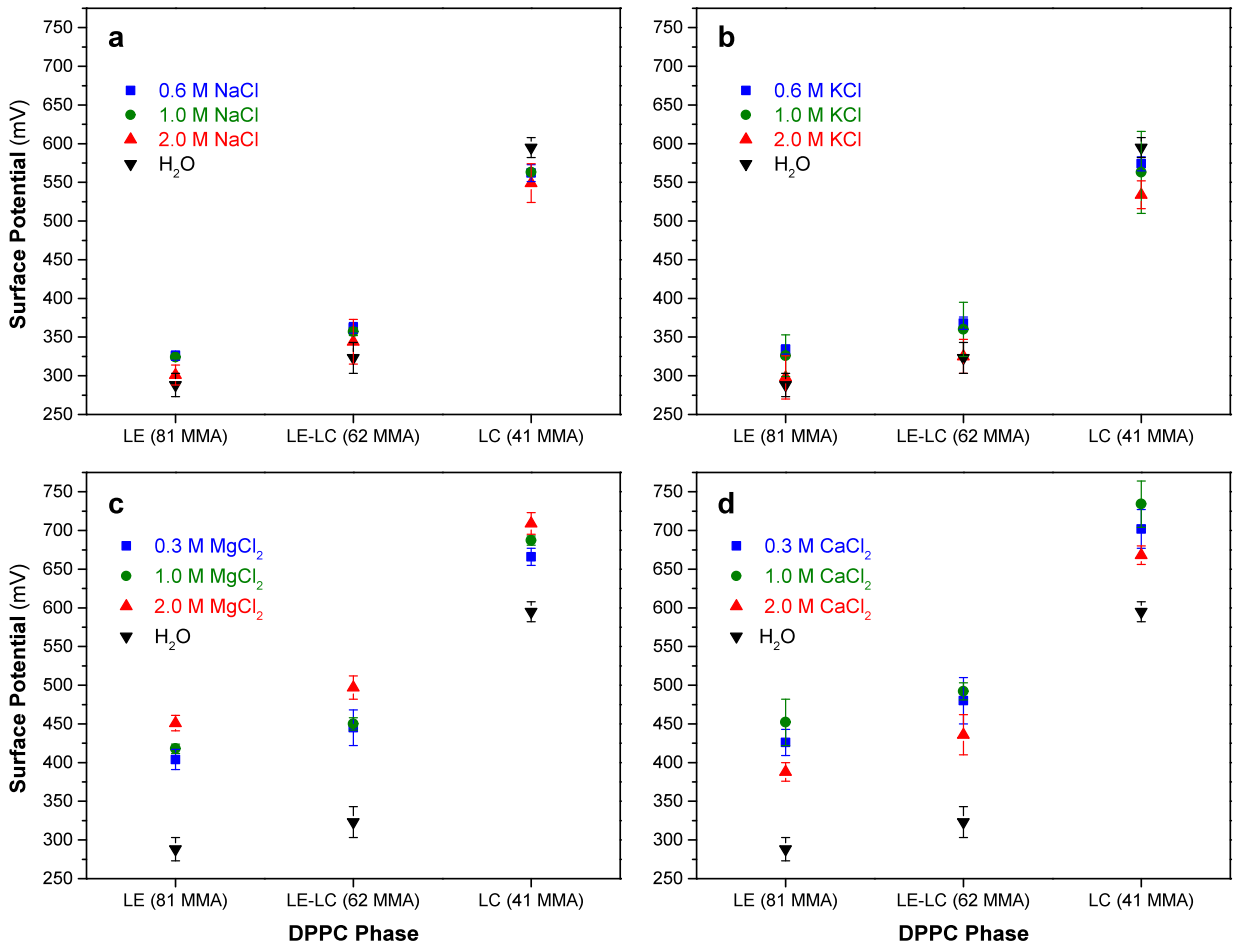

Figure 17. Surface potential for DPPC monolayers on different subphases (a) NaCl, (b) KCl, (c) $MgCl_2$, and (d) $CaCl_2$.

When DPPC head groups lie closer to the interface, it is reasonable to assume that the monolayer will be slightly expanded than that of neat water because it is more difficult for DPPC molecules to pack together. In an expanded monolayer the alkyl tail chains have more rotational freedom. This increases the chances of gauche defects within the chain (parts of the chain that do not adopt a *trans* configuration). It is reasonable to assume then, that μ_{tail} is lowered in an expanded monolayer, since the directions of the tail dipoles are less aligned. This translates to a lowered surface potential value. The last contribution is from the EDL Ψ_0, which is generated in the presence of ions. The formula for Ψ_0 based on Gouy-Chapman theory is given in Eq.(9).

Even though DPPC monolayers has been shown to behave like monolayers with negative surface charge density,[29] it is zwitterionic and assumed to be electrically neutral. Cations may be attracted to the strong dipole created between the phosphate and choline groups in the DPPC head group and this could create an ionic layer below the monolayer. However it is assumed that the contribution from these effects Ψ_0 is relatively small.

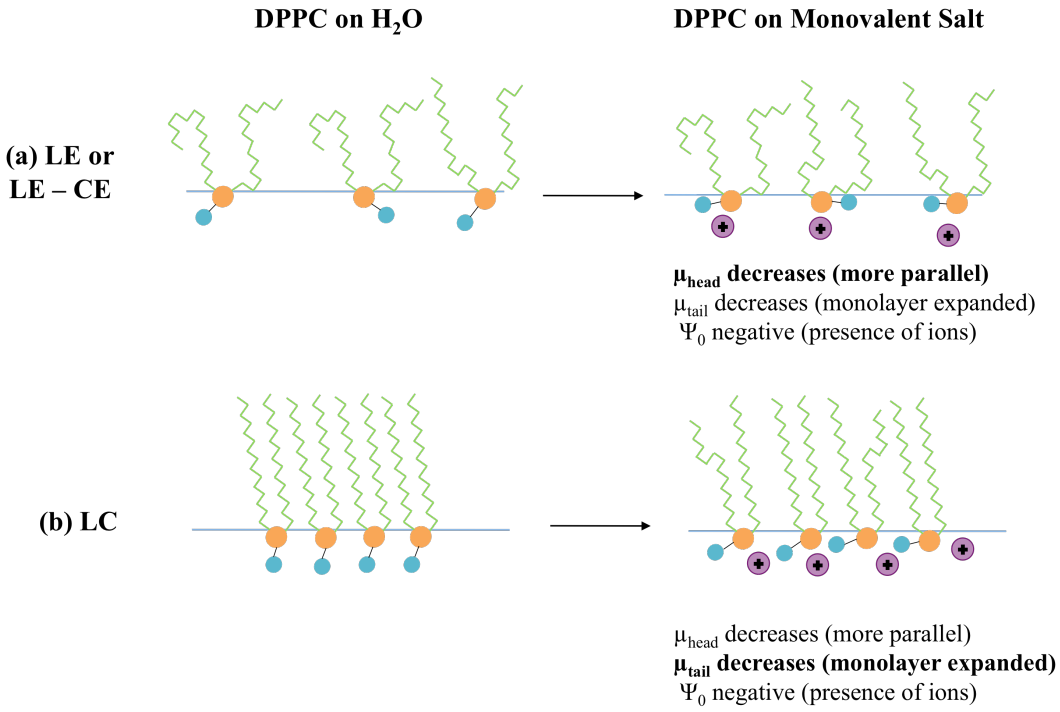

Figure 18. Schematic representation of monovalent effects on DPPC monolayers: (a) Non-condensed phases and (b) liquid-condensed phases.

If one assumes that the change in tail conformations between water and the Na^+/K^+ subphases are negligible, which is reasonable at large mean molecular areas, then the observed surface potential increase seen with monovalent solutions can be attributed to the change in tilt angle of the choline head group.

4.2.2 Surface Potential Contributions in the DPPC LC Phase

In the LC phase, the surface potential of DPPC on neat water was larger than that of DPPC on Na^+/K^+. As in the LE phase, monovalent salts interact with the phosphate head group, causing a change in its conformation. It has been calculated that the head group tilt angle in the LC phase increases from $\theta = 59 \pm 3°$ on neat water to $64 \pm 2°$ on 0.5 M NaCl.[28] As in the case in the LE phase, μ_{head} is then more parallel to the surface and is a positive contribution to the surface potential.

Much like role of the head group in the LE phase, the tails are an important factor in the LC phase, due to the large degree of alignment at high surface pressures. As described in the LE phase, metal ions near the DPPC monolayer cause a reduction in phosphate-choline tilt angle. This causes the monolayer to pack less efficiently, which is of larger importance in the LC phase where surface pressures are higher. The extra room between molecules allows for some gauche defects to occur, resulting in a lower μ_{tail} for DPPC on Na^+/K^+ than that of water. Since the EDL contribution Ψ_0 is expected to be the same between DPPC phases, it is believed that this reduction in μ_{tail} is largely responsible for the observed increased surface potential of DPPC monolayers on monovalent salt subphases.

An attempt at quantifying these effects is possible if the values of μ_{head} and μ_{tail} are known. Nakahara et al. found values of $\mu_{head} = 2.75$ D and $\mu_{tail} = 0.33$ D per tail for DPPC molecules in the LC phase.[30] The contribution to the surface normal of μ_{head} can be found by taking the cosine of the tilt angle. Using the tilt angles mentioned above, the change in dipole contribution to the surface normal $\Delta\mu_{head}$ in going from a neat water surface to a 2.0 M NaCl surface is $\Delta\mu_{head} = 1.20$ D – 1.42 D = − 0.22 D. The total dipole contribution of the tails is $\mu_{tail} = 2 \times 0.33$ D = 0.66 D.

While the change in organization of the tails cannot be calculated in this present work, it is assumed that $\Delta\mu_{tail} \leq \Delta\mu_{head}$ based on the given surface potential data.

4.2.3 Concentration Effects with Na^+/K^+ Salt Subphases

In both the LE and LC phases, 2.0 M Na^+/K^+ showed a significant decrease in surface potential compared to lower concentrations. In the LC phase, this follows the argument given in Section 4.2.2 since 2.0 M would be expected to expand the monolayer further, giving more room for DPPC tail reorganization. However, in the LE phase, this is counterintuitive because it is expected that a further decrease in μ_{head} due to more sodium – phosphate binding would increase the surface potential. It is at this point that Ψ_0 and saturation effects should be considered. However, determining the contributions due to the EDL is complicated since ion size effects are difficult to measure and it is expected that an increase in ion concentration would also affect the monolayer's surface charge density σ. In order to try to assess whether this change in surface potential could be a result from a saturation of ions at the interface, number densities can be approximated. Assuming the surface concentration of ions in the interfacial region is half of that in the bulk and that the interfacial region is uniformly distributed with respect to the ions, the calculated mean ionic area, or the area at the surface in which one expects to find one cation, for a 2.0 M cation solution at the interface (see Appendix) is 83 $Å^2$/cation, this is roughly twice of the expected mean molecular area for DPPC molecules in the LC phase (41 MMA). This suggests that at 2.0 M concentrations of monovalent cations the surface is not saturated.

4.3 Surface Potential Measurements of DPPC Monolayers on Divalent Salt Subphases

The surface potential results for Mg^{2+} and Ca^{2+} are shown in Table 1 and Fig. 17. For both Mg^{2+} and Ca^{2+}, an increase of 70−170 mV in the surface potential with respect to DPPC on neat

water was observed. For Mg^{2+}, the deviation from water increased with concentration. On the other hand, 2.0 M Ca^{2+} showed a smaller increase when compared to the lower concentrations. These surface potential observations are much larger in magnitude than the effects of monovalent salts, suggesting that divalent salts have an increased ability to interact with the phospholipid monolayer.

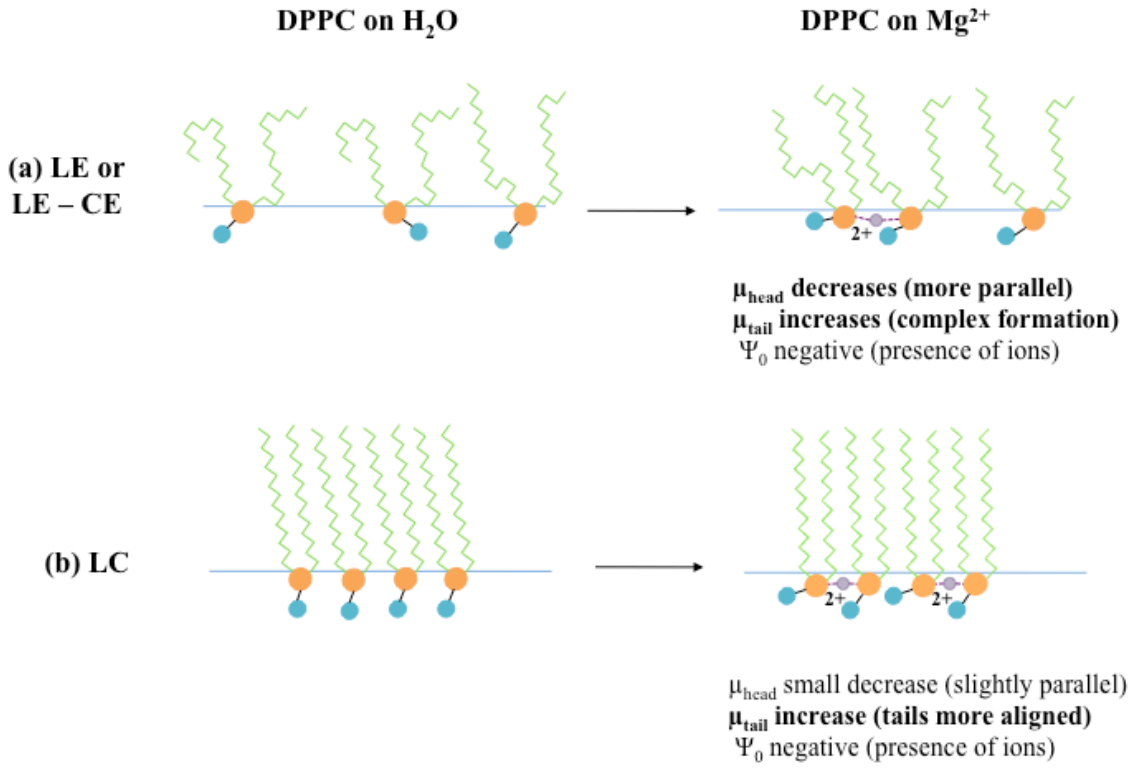

Figure 19. Schematic representation of Mg^{2+} effects on DPPC monolayers: (a) non-condensed phases and (b) liquid-condensed phases.

4.3.1 Surface Potential Contributions in the DPPC LE and LC Phases

The surface potential of DPPC monolayers on an Mg^{2+} subphase was increased along all phases and concentrations. However, Π-*A* isotherms show an expanded monolayer, with the expansion with respect to water increasing with increasing concentration (see Fig. 21 in the

Appendix).[a] A new model for the DPPC monolayer could explain this seemingly conflicting data for Mg^{2+} (Fig. 19).

This model proposes that Mg^{2+} forms a 1:2 complex with DPPC molecules in the monolayer. The magnesium interacts with the headgroups from the phosphate side (much like the monovalent interaction proposed earlier) and this causes the head group to lie more towards the surface. This complexation bridges two DPPC molecules, bringing them closer together.

In the LE phase, the expected changes in monolayer properties would match the observed results: a higher surface potential and expanded monolayer. The dipole of the head group μ_{head} is decreased, as it lies more parallel to the surface. The dipole moments of the tails μ_{tail} would expect to increase because the tails of bridged DPPC molecules hinders tail rotational freedom. Both of these effects serve to increase the surface potential of the monolayer. The packing ability of the monolayer is also reduced, which explains expansion seen in isotherms.

In the LC phase, the ability of this model to explain the observed surface potential values is less plausible. The packing ability of the monolayer would still be reduced which is expected to be much more significant in the LC phase. However, an increase in surface potential with respect to water is observed. These results suggest that Mg^{2+} interact with the DPPC monolayer, but the microscopic mechanism of binding remains unclear. It is possible that Mg^{2+} behaves differently (more monovalent-like or more divalent-like) under different DPPC phases.

4.3.2 Surface Potential Contributions of Ca^{2+} in the DPPC LE and LC Phases

The formation of a 2:1 complex formed between Ca^{2+} and DPPC monolayers has been proposed in literature.[31] However, the observed surface potential values for DPPC on $CaCl_2$ subphases do not fully agree with the proposed bridging model above. The surface potential of

[a] This information was obtained through private communication with Ellen M. Adams.

DPPC on calcium is increased across all concentrations with respect to DPPC on neat water and this could be explained with a reasoning similar to that used for Mg^{2+}. However, the increase of surface potential on 2.0 M $CaCl_2$ is largely reduced. Furthermore, there is evidence that a more complicated effect may be occurring with Ca^{2+}. The Π-*A* isotherms of DPPC on $CaCl_2$ subphases show unchanged lift-off areas with respect to water, suggesting that the head group is not changing orientation. The overall monolayers in these isotherms are condensed in LE and LE-LC phases with respect to neat water, as opposed to the expanded ones seen on Mg^{2+} monolayers (see Figs. 22 and 23 in the Appendix).[a] Since it is thought that divalent cations are interacting with the phosphate in the DPPC head group, it is likely that the hydration shells of each cation play an important role. The differences in size of these shells for Mg^{2+} and Ca^{2+} could lead to different microscopic binding mechanisms, which would be reflected in the macroscopic surface potential value.

[a] This information was obtained through private communication with Ellen M. Adams.

Chapter 5: Conclusions and Future Work

The surface potential of DPPC monolayers on various salt subphases was measured. Monovalent cations Na^+/K^+ showed a small increase in the surface potential with respect to DPPC on neat water. In contrast, the divalent cations Mg^{2+}/Ca^{2+} showed a larger increase in the surface potential. By using models of metal ion interactions with the phosphate group in DPPC, the close relationship between the measured surface potential and the dipole components μ_{head} and μ_{tail} was discussed. It is proposed that the presence of ions changes the headgroup tilt angle of μ_{head} towards the interface, creating a positive contribution to the surface potential and reducing the packing ability of the monolayer. For monovalent cations, it is proposed that μ_{tail} decreases due to the expanded monolayer, which is most clearly seen in the LC phase of DPPC. On the other hand, μ_{tail} is proposed to increase when divalent salts bind to DPPC. This is due to a 2:1 complex in which a divalent ion "bridges" two DPPC molecules, expanding the monolayer but providing more alignment of the alkyl tails. Both the surface potential data and Π-*A* isotherm data of DPPC monolayers on Mg^{2+} subphases agree well with this model. However, Ca^{2+} agree only partially with the surface potential data presented. It is suggested that the discrepancy with DPPC monolayers on Ca^{2+} and Mg^{2+} stems from differences in hydration shell radii and mechanisms of binding, which could lead to a different type of complex formed between Ca^{2+} and DPPC.

However, this study is only a first step into elucidating the organization of DPPC monolayers. More concrete evidence of the models proposed can be obtained if surface potential and surface pressure-area isotherms can be collected simultaneously. The data obtained from these two surface techniques can be complemented by other experimental methods such as BAM, which can observe ion effects on the domain morphology of DPPC, and VSFG spectra,

from which the ion binding to the phosphate group can be directly studied. In addition, calculations involving the Demchak-Fort model mentioned in Chapter 2 with experimental surface potential data could serve to validate changes in the dipole moments μ_{head} and μ_{tail}.

The results presented here have implications for the marine aerosols. Using DPPC as a surrogate for the organic layer found on marine aerosols, this study investigated the organizational changes due to salt, which is ubiquitous in the ocean. Many of the interpretations proposed above involve an expanded monolayer, which translates to a more diffuse boundary. This allows more gas exchange between the atmosphere and the monolayer, increases the likelihood of evaporation water from the aerosol, and facilitates the interfacial transport of many atmospheric relevant species such as halides and sulfuric acid.[5] Furthermore, the organization of dipoles and charges on the surface of aerosols can affect their ability to electrify thunderclouds[32] and to act as cloud condensation nuclei. All of these processes can have an impact on Earth's changing climate.

References

1. Boucher, O. et al. in Climate Change 2013: The Physical Science Basis. Contribution of Working Group I to the Fifth Assessment Report of the Intergovernmental Panel on Climate Change (Cambridge University Press).
2. Finlayson-Pitts, B. J. & Pitts, Jr., J. N. Chemistry of the Upper and Lower Atmosphere. (Academic Press, 2000).
3. Cunliffe, M. et al. Sea Surface Microlayers: A Unified Physicochemical and Biological Perspective of the Air-Ocean Interface. Prog. Oceanogr. **109,** 104–116 (2013).
4. Rinaldi, M. et al. Primary and Secondary Organic Marine Aerosol and Oceanic Biological Activity: Recent Results and New Perspectives for Future Studies. Adv. Meteorolgy 1–10 (2010).
5. Donaldson, D. . & Vaida, V. The Influence of Organic Films at the Air-Aqueous Boundary on Atmospheric Processes. Chem. Rev. **106,** 1445–1461 (2006).
6. Hawkins, L. N. & Russel, L. M. Polysaccharides, Proteins, and Phytoplankton Fragments: Four Chemically Distinct Types of Marine Primary Organic Aerosol Classified by Single Particle Spectromicroscopy. Adv. Meteorolgy (2010).
7. Ellison, G. B. Atmospheric Processing of Organic Aerosols. J. Geophys. Res. **104,** 11,633–11,641 (1999).
8. Tervahattu, H. et al. New Evidence of an Organic Layer on Marine Aerosols. J. Geophys. Res. **107,** AAC1–8 (2002).
9. Espinosa, L. F., Pantoja, S., Pinto, L. A. & Rullkötter, J. Water Column Distribution of Phospholipid - Derived Fatty Acids of Marine Microorganisms in the Humboldt Current System off Northern Chile. Deep-Sea Res. Part II-Top. Stud. Oceanogr. **56,** 1063–1072 (2009).
10. Close, H. G., Wakeham, S. G. & Pearson, A. Lipid and 13C Signatures of Submicron and Suspended Particulate Organic Matter in the Eastern Tropical North Pacific: Implications for the Contribution of Bacteria. Deep-Sea Res. Part - Oceanogr. Res. Pap. **85,** 15–34 (2014).
11. Brandsma, J. et al. Spatial Distribution of Intact Polar Lipids in North Sea Surface Waters: Relationship with Environmental Conditions and Microbial Community Composition. Limnol. Oceanogr. **57,** 959–973 (2012).
12. Barzyk, W. & Vuorinen, J. Applications of the Vibrating Plate (VP) Technique to Measuring Electric Surface Potential, ΔV, of Solutions; the Flow Cell for Simultaneous Measurement of the ΔV and the Surface Pressure, ∏. Colloids Surf. Physicochem. Eng. Asp. 1–10 (2011).
13. Kirk, D. . & Foulkes, F. . An Ionized Air Reference Electrode: II. Applications. J. Electrochem. Soc. **131,** 1332–1336 (1984).
14. Brockman, H. Dipole Potential of Lipid Membranes. Chem. Phys. Lipids **73,** 57–59 (1994).
15. Gaines Jr., G. L. Insoluble Monolayers at Liquid-Gas Interfaces. (Interscience, 1966).
16. Helmholtz, H. Studien über electrische Grenzschichten. Ann. Phys. Chem. **7,** 337–382 (1879).
17. Taylor, D. M., Oliveira Jr., O. N. & Morgan, H. Models for Interpreting Surface Potential Measurements and Their Application to Phospholipid Monolayers. J. Colloid Interface Sci. **139,** 508–518 (1990).
18. Demchak, R. J. & Fort Jr., T. Surface Dipole Moments of Close-Packed Un-ionized Monolayers at the Air-Water Interface. J. Colloid Interface Sci. **46,** 191–202 (1974).

19. Dynarowicz-Łatka, P., Cavalli, A., Silva Filho, D. A., dos Santos, M. . & Oliveira Jr., O. N. Dipole Moments in Langmuir Monolayers from Aromatic Carboxylic Acids. Chem. Phys. Lett. **326,** 39–44 (2000).
20. Vögel, V. & Möbius, D. Hydrated Polar Groups in Lipid Monolayers: Effective Local Dipole Moments and Dielectric Properties. Thin Solid Films **159,** 73–81 (1988).
21. Gaines Jr., G. L. in Insoluble Monolayers at Liquid-Gas Interfaces 136–208 (Interscience, 1966).
22. Hua, W., Verreault, D., Adams, E. M., Huang, Z. & Allen, H. C. Impact of Salt Purity on Interfacial Water Organization Revealed by Conventional and Heterodyne-Detected Vibrational Sum Frequency Generation Spectroscopy. J. Phys. Chem. C **117,** 19577–19585 (2013).
23. Finlayson, A. . The pH Range of the Mohr Titration for Chloride Ion Can Be Usefully Extended to 4-10.5. J. Chem. Educ. **69,** 559 (1992).
24. Millero, F. J. Chemical Oceanography. (CRC Press, 2006).
25. Jyoti, A. et al. An Investigation of the Compression Rate Dependence on the Surface Pressure-Surface Area Isotherm for a Dipalmitoyl Phosphatyidylcholine Monolayer at the Air/Water Interface. Colloids Surf. Physicochem. Eng. Asp. **116,** 173–180 (1996).
26. Salay, L. C., Ferreira, M., Oliveira Jr., O. N., Nakaie, C. R. & Schreier, S. Headgroup Specificity for the Interaction of the Antimicrobial Peptide Tritrpticin with Phospholipid Langmuir Monolayers. Colloids Surf. B Biointerfaces **100,** 95–102 (2012).
27. Griesbauer, J., Bössinger, S., Wixforth, A. & Schneider, M. . Simultaneously Propagating Voltage and Pressure Pulses in Lipid Monolayers of Pork Brain and Synthetic Lipids. Phys. Rev. E **86,** 061909–1–5 (2012).
28. Casillas - Ituarte, N. N., Chen, X., Castada, H. & Allen, H. C. Na+ and Ca2+ Effect on the Hydration and Orientation of the Phosphate Group of DPPC at Air-Water and Air-Hydrated Silica Interfaces. J. Phys. Chem. B **114,** 9485–9495 (2010).
29. Chen, X., Hua, W., Huang, Z. & Allen, H. C. Interfacial Water Structure Associated with Phospholipid Membranes Studied by Phase-Sensitive Vibrational Sum Frequency Generation Spectroscopy. J. Am. Chem. Soc. **132,** 11336–11342 (2010).
30. Nakahara, H. et al. Cerbroside Langmuir Monolayers Originated from the Echinoderms I. Binary Systems of Cerebrosides and Phospholipids. Colloids Surf. B Biointerfaces **42,** 157–174 (2005).
31. Sovago, M., Wurpel, G. W. H., Smits, M., Müller, M. & Bonn, M. Calcium-Induced Phospholipid Ordering Depends on Surface Pressure. J. Am. Chem. Soc. **129,** 11079–11084 (2007).
32. Jungwirth, P., Rosenfeld, D. & Buch, V. A possible new molecular mechanism of thundercloud electrification. Atmospheric Res. **76,** 190–205 (2005).

Appendix

DPPC Isotherms on Water and Salt Subphases

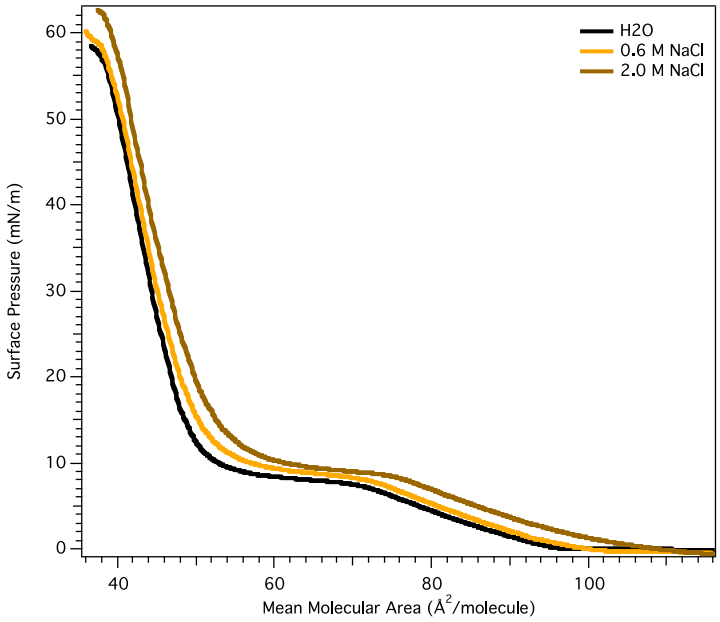

Figure 20. Π-*A* isotherms of DPPC monolayers on NaCl subphases (collected by Ellen M. Adams).

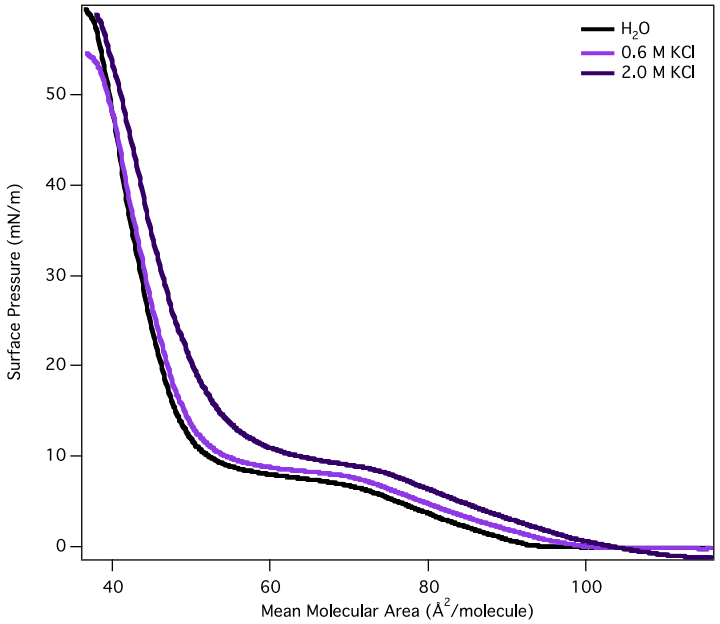

Figure 21. Π-*A* isotherms of DPPC monolayers on KCl subphases (collected by Ellen M. Adams).

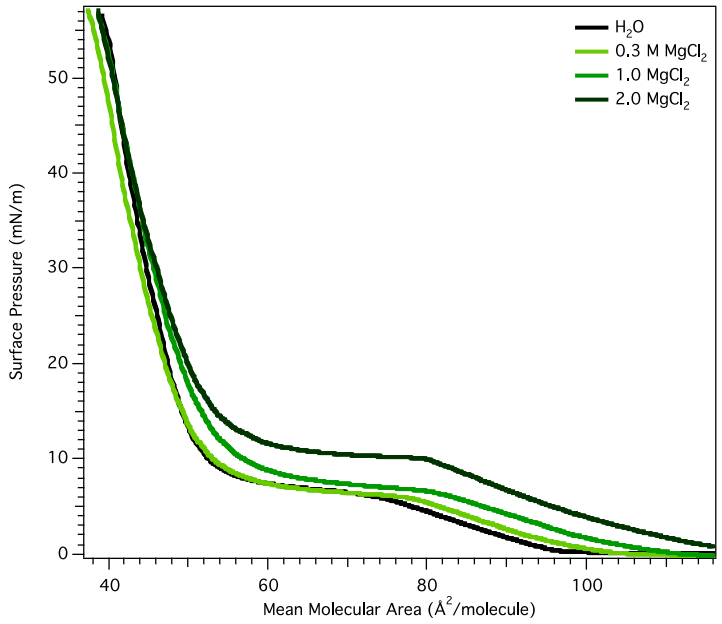

Figure 22. Π-*A* isotherms of DPPC monolayers on $MgCl_2$ subphases (collected by Ellen M. Adams).

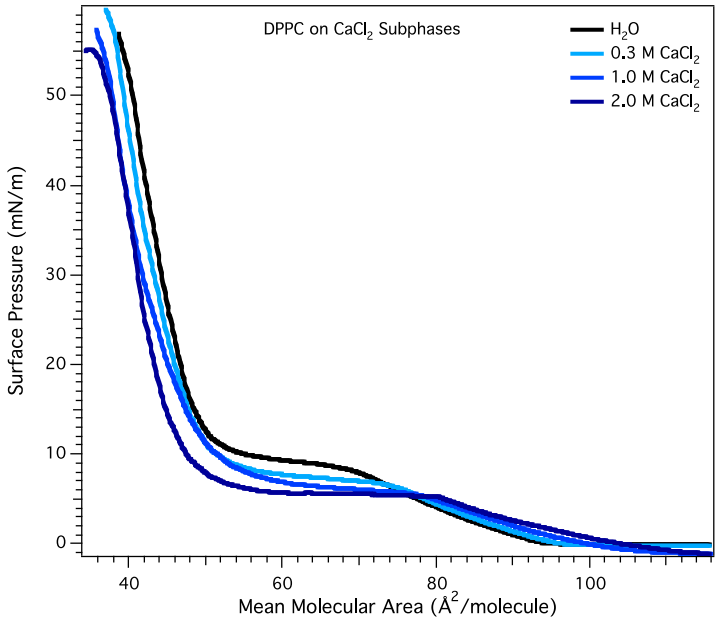

Figure 23. Π-*A* isotherms of DPPC monolayers on $CaCl_2$ subphases (collected by Ellen M. Adams).

Calculations of the Mean Ionic Area (MIA)

Assumptions

Interfacial depth of 20 Å

Surface concentration of ions = half of concentration in bulk

Mean molecular area of DPPC in LC phase = 41 $Å^2$/molecule

Ions in the interfacial region are uniformly distributed.

Quantities

Surface area of cell used = 3872 mm^2 = 3.872×10^{17} $Å^2$

For 2.0 M NaCl, there are

$$\frac{2.0\text{ mol NaCl}}{1\ L}\times 0.03872\ L\times N_A = 4.66\times10^{22}\,\text{Na}^+\text{ in the bulk} = 2.33\times10^{22}\,\text{Na}^+\text{ at the surface}$$

Then, the amount of Na^+ in a 20 Å layer is:

$$\frac{2.33\times10^{22}\,\text{Na}^+}{1\times10^{8}\,Å\text{ (cell depth)}}\times 20Å = 4.66\times10^{15}\,\text{Na}^+$$

Then dividing by the surface area of the cell and inverting gives the area in which a single Na^+ ion is found:

$$MIA = \left(\frac{4.66\times10^{15}\,\text{Na}^+}{3.87\times10^{17}\,Å^2}\right)^{-1} = 83\frac{Å^2}{\text{Na}^+}$$